Estimating the Turn-Around Radii of Six Isolated Galaxy Groups in the Local Universe

Jounghun Lee

Astronomy Program, Department of Physics and Astronomy, Seoul National University, Seoul 08826, Republic of Korea

jounghun@astro.snu.ac.kr

ABSTRACT

The estimates of the turn-around radii of six isolated galaxy groups in the nearby universe are presented. From the Tenth Data Release of the Sloan Digital Sky Survey, we first select those isolated galaxy groups at redshifts $z \leq 0.05$ in the mass range of $[0.3\text{-}1]\times10^{14}\,h^{-1}M_{\odot}$ whose nearest neighbor groups are located at distances larger than fiften times their virial radii. Then, we search for a gravitationally interacting web-like structure around each isolated group, which appears as an inclined streak pattern in the anisotropic spatial distribution of the neighbor field galaxies. Out of 59 isolated groups, only seven are found to possess such web-like structures in their neighbor zones, but one of them turns out to be NGC 5353/4, whose turn-around radius was already measured in the previous work and thus excluded from our analysis. Applying the Turn-around Radius Estimator algorithm devised by Lee et al. to the identified web-like structures of the remaining six target groups, we determine their turn-around radii and show that three out of the six targets have larger turn-around radii than the spherical bound limit predicted by the Planck cosmology. We discuss possible sources of the apparent violations of the three groups, including the underestimated spherical bound-limit due to the approximation of the turn-around mass by the virial mass.

Subject headings: cosmology:theory — large-scale structure of universe

1. Introduction

When a dark matter (DM) halo forms in the universe, its gravitational struggle against the Hubble expansion in its linear stage leaves behind a unique vestige that is hardly effaced by any nonlinear complications in the subsequent evolution. This vestige, called the turnaround radius, reflects the very moment when the radial velocity of a proto-halo begins to change its sign as its self-gravity catches up with the Hubble flow. The merit and power of this vestige resides in the fact that even though it is a local quantity, it can be sufficiently well modeled by the linear physics. If the turn-around radii of DM halos be directly estimated from observations, then the comparison of the estimated values with the model predictions would put a new constraint on the initial conditions of the universe (Pavlidou & Tomaras 2014; Pavlidou et al. 2014).

The linear physics predicts that in an accelerating phase of the universe the turn-around radii, r_t , of DM halos are bounded by a finite upper limit, $r_{t,u}$, whose value sensitively depends on the amount and equation of state of dark energy (DE) (Pavlidou & Tomaras 2014). In the standard picture where DE is given as the cosmological constant Λ and DM is cold (i.e, Λ CDM cosmology), the upper bound limit of the turn-around radii is given as

$$r_{t,u} = f \left(\frac{GM}{\Omega_{\Lambda} H^2}\right)^{1/3} \,, \tag{1}$$

where H is the Hubble parameter, Ω_{Λ} is the density parameter of Λ , M is the turn-around mass (i.e., the mass of a spherical region enclosed by the turn-around radii r_t) and f is a parameter introduced to account for the effect of asymmetry in the DM distribution of a halo (Pavlidou & Tomaras 2014).

According to the linear physics which precludes an individual halo from having $r_t \geq r_{t,u}$ (i.e., bound-limit violation) in the Λ CDM cosmology, f has an exact value of unity only if a DM halo forms through spherical collapse process (Pavlidou & Tomaras 2014). For the more realistic case of non-sperhcal DM distributions, the value f has been estimated to be approximately 1.5 on the whole mass scale (see Figure 1 in Pavlidou & Tomaras 2014). This value of $f \approx 1.5$, however, is the empirical value obtained from the numerical simulations unlike the case of the spherical symmetry. Given that the degree of the deviation of the DM distribution from the spherical symmetry varies from halos to halos, the parameter f for the non-spherical bound limit should be regarded as a stochastic variable and the empirically obtained value of 1.5 as an average of this stochastic variable. Hence, the stochastic nature of the parameter f implies that it should be possible for individual halos with non-spherical DM distributions to violate the spherical bound limit on rare occasions since the spherical bound limit is 1.5 times lower on average than the non-spherical counterpart.

Lee & Li (2017) numerically examined whether or not this theoretical prediction derived purely from the linear physics is valid in the deeply nonlinear regime. Directly measuring the mean turn-around radii averaged over sample halos on various mass scales from the MultiDark Planck simulations (Klypin et al. 2016), they confirmed that the mean turn-around radius never exceeds both of the spherical and the non-spherical bound limits (say, $r_{t,u}^{(s)}$ and $r_{t,u}^{(ns)}$, respectively) on the whole mass scale. Lee & Li (2017) also explored the

probability of finding an individual DM halo with $r_t \geq r_{t,u}^{(s)}$ and found that 14% of DM halos with masses equal to or larger than $10^{13}\,h^{-1}M_{\odot}$ violate the spherical bound limit in a Planck cosmology (Planck Collaboration et al. 2014). Besides, their analysis revealed that in a modified gravity (MG) model where the notion of DE is replaced by the deviation of the gravitational law from the general relativity (e.g., Joyce et al. 2015, and references therein), the frequency of the occurrences of the spherical bound limit violations becomes elevated, which indicated that it should be in principle possible to test the gravitational law on the cosmological scale by exploring the rareness of the spherical bound limit violations.

As mentioned in Pavlidou & Tomaras (2014), the optimal targets for the observational inspection of the bound limit violations are not the clusters but the groups of galaxies, especially those located in the low-density environment. It is because Equation (1) was derived under the assumption that a DM halo already reaches a complete relaxation state, which can be hardly justified for the case of the galaxy clusters. Despite that the detections of a couple of bound violating cluster and supercluster were reported by the previous works (e.g., Karachentsev et al. 2014; Pearson et al. 2014), the detections did not attract much attention, as it was suspected that the apparent violations of the spherical bound limit by those cluster and supercluster could be ascribed to the deviation of their dynamical states from complete relaxation and/or large uncertainties associated with the estimates of their turn-around radii from the peculiar velocities of their neighbor galaxies.

A practical difficulty to detect the bound-limit violations on the group scale stems from the following fact: Since the galaxy groups have much weaker gravitational influences on their neighbor galaxies than the galaxy clusters, the conventional methodology based on the direct measurements of the peculiar velocity profile (e.g., see Karachentsev et al. 2014) is likely to fail in properly estimating the turn-around radii of galaxy groups. Recently, Lee et al. (2015b) developed an efficient practical algorithm dubbed the Turn-around Radius Estimator (TRE) which does away with the measurements of the peculiar velocities unlike the conventional methodology. The applicability of the TRE, however, is contingent upon the existence of gravitationally interacting filament or sheet-like structure around a target object.

Lee et al. (2015b) applied the TRE to NGC 5353/4, a nearby isolated galaxy group around which a thin straight filamentary structure had already been detected (Kim et al. 2016), and showed that the turn-around radius of NGC 5353/4 seemed to exceed the spherical bound limit set by the Planck Λ CDM cosmology (Planck Collaboration et al. 2014). This was the first observational detection of an occurrence of the spherical bound-limit violation on the galaxy group scale. A detection of a single group which appears to violate Equation (1) with f=1, however, cannot shatter down the Λ CDM cosmology, due to the stochastic

nature of the parameter f, as mentioned in the above. It is necessary to apply the TRE to a larger sample of galaxy groups and to statistically and systematically explore the frequency of the occurrences of the spherical bound limit violations, which we attempt to conduct in this paper.

The upcoming sections will present the followings: a concise review of the TRE in Section 2; the estimates of the turn-around radii of the nearby isolated galaxy groups via the TRE and the frequency of the occurrences of the bound limit violation on the group scale in Section 3; a summary of the results and the discussions of the physical implications in Section 4.

2. A Brief Review of the TRE Algorithm

The TRE algorithm is based on the numerical discovery of Falco et al. (2014) that the following universal formula depicts well the radial velocity profile, $v_r(r)$, of DM particles in the bound zone around a halo with virial radius r_v :

$$\frac{v_r(r)}{H} = r - a \frac{V_v}{H} \left(\frac{r}{r_v}\right)^{-b} \,, \tag{2}$$

where the bound-zone corresponds to the radial distances from the halo center, r, in the range of $(3-8)r_v$, H is the Hubble parameter, and V_v is the central velocity at r_v . Falco et al. (2014) determined empirically the amplitude and slope parameters, a and b, of Equation (2) with the help of a N-body simulation and suggested that the best-fit values of a and b should be universal, independent of mass scales and redshifts. According to their claim, once the amplitude and slope parameters are set at the universal values, it is possible to estimate the value of r_v (or equivalently, virial mass M_v) of a given halo by adjusting Equation (2) to the observed radial velocity profile.

Pointing out that neither v_r nor r in Equation (2) is directly observable, Falco et al. (2014) brought up the following heutristic scheme via which Equation (2) could be put into practice. Provided that a target halo is surrounded by a web-like structure (i.e., either a filament-like or a sheet like structure) of DM in its bound zone, it is possible to express Equation (2) in terms of the observables:

$$l_z = \frac{r_{2d}}{\tan \beta} - a \cos \beta \frac{V_v}{H} \left(\frac{r_{2d}}{\sin \beta r_v}\right)^{-b}, \tag{3}$$

where $l_z \equiv cz/H$ with relative redshift z and speed of light c, r_{2d} is the radial separation distance from the halo center in the projected plane of sky orthogonal to the sightline toward

the target halo and β is the angle between the position vector from the halo center and the sightline. Given that both of r_{2d} and z are readily observable, it can be said that Equation (3) is a practical version of Equation (3) which has an additional parameter β as a trade-off. In other words, when Equation (3) is fitted to the observed radial velocity profile by adjusting the value of M_v , the angle β takes on a nuisance parameter, whose presence would unavoidably enlarge the associated statistical errors on M_v (see also Lee et al. 2015a).

Having a practical version of Equation (2), however, does not ensure a success in its application to real observational data. It was necessary to test whether or not the radial velocity profile obtained not from DM particles but from luminous galaxies in the bound zone through anisotropic averaging would be well described by the same universal formula as Equation (3). In addition, it was also necessary to prove the claim of (Falco et al. 2014) about the universality of the slope and amplitude parameters, a and b, in Equations (2) and (3).

Several numerical works that were conducted in light of Falco et al. (2014) consolidated the usefulness of Equations (2) and (3) by using larger samples from higher-resolution N-body simulations. For instance, Lee (2016) proved by analyzing the data from the Millennium Run II simulations (Boylan-Kolchin et al. 2009) that even when the radial velocity profile was obtained not from DM particles but from the galaxy-size halos, the same analytic formula as Equation (2) still validly described the numerical result. Yet, they noted that the best-fit values of a and b do not show universal constancy but exhibit variance from halos to halos, implying that not only β but also a and b should be treated as nuisance parameters in Equation (3). Lee & Yepes (2016) confirmed by analyzing the data from the Multidark Planck simulations (Klypin et al. 2016) that Equation (2) worked even when the bound-zone radial velocity profile was constructed not through the isotropic averaging but through the anisotropic averaging over the filaments or sheets. Very recently, Albaek et al. (2017) showed that the baryonic processes would not alter severely the functional form of the bound-zone radial velocity profiles.

The key idea of Lee et al. (2015b) who devised the TRE algorithm is that Equation (2) can be used to mimic the expansion of a proto-halo until the turn-around moment. A proto-halo expands at a slower rate than the Hubble flow due to its self-gravity before the turn-around moment (t_t) . Claiming that the radial velocity profile of a proto-group before t_t may be well described by the same formula as Equation (2), Lee et al. (2015b) suggested that Equation (2) should become equal to zero at the turn-around radius (r_t) :

$$r_t = a \frac{V_v}{H} \left(\frac{r_t}{r_v}\right)^{-b} . {4}$$

The procedure to estimate the value of r_t of a massive object via the TRE algorithm can

be summarized as follows (for a detailed description, see Lee et al. 2015b): (1) For a galaxy group or cluster whose viral mass M_v is already known from priors, search for a filament-like or sheet-like (collectively called, web-like) structure in its neighbor zone; (2) Construct the radial velocity profile along the identified web-like structure; (3) Fit the constructed radial velocity profile to Equation (3) by adjusting the values of a, b and β : (4) Put the best-fit values of a and b into Equation (4) and find a solution to it. In Section 3, we will refine further this TRE algorithm and present a useful formula for the evaluation of the marginalized errors on the estimates of the turn-around radii.

3. Turn-Around Radii of the Sloan Galaxy Groups

Tempel et al. (2014) applied a redshift-space adapted version of the friends-of-friends (FoF) algorithm to the galaxy sample from the Tenth Data Release of the Sloan Digital Sky Survey (SDSS DR10) (Ahn et al. 2014) to obtain a catalog of the FoF groups. From the catalog, one can draw out information on various properties of the FoF groups including the redshifts (z), equatorial coordinates of their centers (RA and DEC), and their virial radii (r_v) and masses (M_v) which were estimated under the assumption that their DM density profiles follow the Navvaro-Frenk-White (NFW) formula (Navarro et al. 1997). They also provided the galaxy catalog from which information on the spectroscopic properties of the member galaxies belonging to each FoF group can be extracted.

Analyzing the group catalog of Tempel et al. (2014), we select those FoF groups with $0.3 \leq M_v/(10^{14}h^{-1}M_{\odot}) \leq 1$ (typical group scale) and $z \leq 0.05$, being isolated enough to be separated by their nearest groups of comparable masses by more than $15r_v$. We consider only the isolated groups, given the numerical result of Lee & Yepes (2016) that the best agreement between Equation (2) and the reconstructed radial velocity profile is achieved for the case of the isolated halos. Furthermore, the TRE algorithm substitutes M_v for the turnaround mass in Equation (1), which approximation works best for the case of an isolated object.

Selected are a total of 59 isolated galaxy groups, in the neighbor zones of which we attempt to identify web-like structures composed of the field galaxies. Although in the previous works of Falco et al. (2014) and Lee (2017), the neighbor zone around a cluster was defined to have a large extent of $|l_z| \leq 40 \, h^{-1} {\rm Mpc}$ and $4 \leq r_{2d}/(h^{-1} {\rm Mpc}) \leq 20$, we confine the neighbor zone to a much smaller extent of $|l_z| \equiv |cz/H| \leq 20 \, h^{-1} {\rm Mpc}$ and $2 \leq r_{2d}/(h^{-1} {\rm Mpc}) \leq 10$, given that the target objects are not the clusters but the less massive groups whose gravitational influences can reach out only this small extent. It is also worth explaining here why we identify a web-like structure from the distributions only

of the *field* galaxies, excluding the wall galaxies. It is because the wall galaxies unlike the field counterparts are expected to be heavily influenced by their own hosts even if they are located in the same neighbor zone.

Adopting the methodology suggested by Falco et al. (2014) for the identification of the web-like structures, we first look for the overdense pixels in the neighbor zone around each isolated group by counting the field galaxies. The neighbor zone around each isolated group is partitioned into 80 pixels of equal sizes in two dimensional space spanned by r_{2d} and l_z , as illustrated in the left panel of Figure 1. The spherical shell, with inner and outer radii of $2 h^{-1}$ Mpc and $10 h^{-1}$ Mpc, respectively, are also partitioned into eight wedges (say, $\{W_i\}_{i=1}^8$), as depicted in the right panel of Figure 1, where (x,y) denotes a two dimensional position vector from the group center in the equatorial coordinate system, with $r_{2d} = (x^2 + y^2)^{1/2}$. Each wedge represents a realization of the neighbor zone of a given isolated group, and the eight wedges form an ensemble over which the average residual number densities of the neighbor field galaxies around the group will be evaluated.

From the galaxy sample from the SDSS DR10, we select those field galaxies which belong to the neighbor zone of each isolated group by estimating the values of r_{2d} and l_z . Then, we investigate to which pixel and to which wedge each of the neighbor field galaxies belong. Suppose that one wants to find the dimensionless residual number density of the neighbor field galaxies at the ij th pixel of the wedge W_1 (say, $\delta_{ij}^{W_1}$). The first step is to compute the number densities of the neighbor field galaxies belonging to the ijth pixel of the wedge W_1 . The second step is to compute the number densities of the neighbor field galaxies at the same pixel of five different wedges, W_3 , W_4 , W_5 , W_6 , W_7 . Two wedges, W_2 and W_8 , adjacent to the wedge W_1 (see the right panel of Figure 1) are excluded. The third step is to compute the back ground number density of the neighbor field galaxies at the ijth pixel by taking the average over the five wedges.

The fourth step is to evaluate the residual number density at the ijth pixel of the wedge W_1 , δ^1_{ij} , by dividing the difference in the results between the first and the third steps by the background number density at the ijth pixel. The fifth step is to compute the standard deviation, $\sigma^{W_1}_{ij}$, of the residual number density, in a similar manner. The final step is to see whether or not the condition of $\delta^{W_1}_{ij} \geq \sigma^{W_1}_{ij}$ is met at the ijth pixel of the wedge W_1 . If met, the ijth pixel of the wedge W_1 is selected as a candidate overdense site where a web-like structure composed of the neighbor field galaxies may be found. Retake this procedure repeatedly for the other pixels and wedges to find all the overdense sites in the neighbor zone of each isolated group. See Falco et al. (2014) for a detailed description.

Before proceeding to identify a web-like structure in the overdense pixels of the neighbor zone around each isolated group, it is worth emphasizing that the TRE algorithm would be applicable only to those pixels which would appear altogether as inclined streak lines in the r_{2d} - l_z configuration space, as explained in Brinckmann et al. (2016). Figure 2 plots the analytic formula of Equation (3) for six different cases of β , setting M_v at $5 \times 10^{13} h^{-1} M_{\odot}$. We look for a web-like structure composed of the field galaxies located in the neighbor zone around a target group, which would appear similar to the inclined lines shown in Figure 2.

We find that only seven out of the 59 isolated groups possess such web-like structures in their neighbor zones. Among the seven groups, one turns out to be NGC 5353/4, whose turn-around radius was already estimated by Lee et al. (2015b) to exceed the spherical bound limit. NGC 5353/4 being excluded, the rest six groups (say, GG1, GG2, GG3, GG4, GG5, GG6) become our target groups to which the TRE algorithm is going to be applied for the estimation of their turn-around radii. Table 1 presents the equatorial coordinates, redshifts and virial masses of the six target groups.

Figure 3 shows as red closed circles the locations of the neighbor field galaxies belonging to the overdense pixels around GG1 in the two dimensional configuration space spanned by r_{2d} and l_z . The green dotted line correspond to the locations at which the condition of $l_z = r_{2d}$ is met, while the blue closed circles represent the configurations of the member galaxies of GG1. Noting the existence of an inclined streak of the neighbor field galaxies in the overdense pixels of the wedge W_6 , which look similar to the inclined lines shown in Figure 2, it is identified a web-like structure around GG1 and shown as black open circles in Figure 3. Figures 4-8 show the same as Figure 3 but for the other five target groups. As can be seen, the web-like structures around GG2, GG3, GG4, GG5, GG6 are identified in the wedges of W_8 , W_7 , W_4 , W_2 , W_4 , respectively. Figure 9 shows the same as Figures 3-8 but for the case of an isolated group around which no web-like structure is identified and thus not selected as a target.

Suppose that we identify a web-like structure composed of n_f neighbor field galaxies from one of the eight wedges around a target group. Employing the maximum likelihood method as Lee et al. (2015b) and Lee (2017) did, we determine the best-fit values of a, b, β in Equation (3), which maximizes the following posterior distribution:

$$p(a,b,\beta) \propto \exp\left[-\frac{\chi^2(a,b,\beta)}{2}\right],$$
 (5)

$$\chi^{2}(a,b,\beta) = \sum_{k=1}^{n_{f}} \left[l_{z,k} - l_{z,k}^{T}(a,b,\beta) \right]^{2}, \qquad (6)$$

$$l_{z,k}^{T}(a,b,\beta) = \frac{r_{2d,k}}{\tan \beta} - a\cos \beta \frac{V_v}{H} \left(\frac{r_{2d,k}}{\sin \beta r_v}\right)^{-b}, \qquad (7)$$

where $(r_{2d,k}, l_{z,k})$ are the observed position vector of the kth neighbor field galaxy belonging

to an identified web-like structure, while $l_{z,k}^T$ represents Equation (3) with r_{2d} set at $r_{2d,k}$.

To improve the efficiency of the TRE algorithm in its practical application, we rearrange the terms of Equation (4) to derive the following closed analytic expression for r_t as a function of a and b:

 $r_t(a,b) = \exp\left\{\frac{1}{(1+b)}\ln\left[r_v^b\left(\frac{aV_v}{H}\right)\right]\right\}. \tag{8}$

Suppose that the posterior function, Equation (5), is found to reach its maximum at $a = \hat{a}$, $b = \hat{b}$, $\beta = \hat{\beta}$. Putting the best-fit values, \hat{a} and \hat{b} , into Equation (8), one can readily estimate the turn-around radius of a target group as $\hat{r}_t(\hat{a}, \hat{b})$.

We estimate the associated errors on \hat{r}_t , σ_{r_t} , according to the error propagation formula (Wall & Jenkins 2012):

$$\sigma_{r_t}^2 \approx \left(\frac{\partial r_t}{\partial a}\right) \Big|_{\hat{a},\hat{b}}^2 \sigma_a^2 + \left(\frac{\partial r_t}{\partial b}\right) \Big|_{\hat{a},\hat{b}}^2 \sigma_b^2 + 2\left(\frac{\partial r_t}{\partial a}\right) \Big|_{\hat{a},\hat{b}} \left(\frac{\partial r_t}{\partial b}\right) \Big|_{\hat{a},\hat{b}} \cos(a,b), \tag{9}$$

where σ_a and σ_b denote the marginalized errors in the determination of the best-fit values of a and b, respectively, and cov(a, b) is the marginalized covariance between a and b, three of which can be calculated as

$$\sigma_a^2 = \int d\beta \int da \int db \, (a - \langle a \rangle)^2 \, p(a, b, \beta) \,, \tag{10}$$

$$\sigma_b^2 = \int d\beta \int da \int db \, (b - \langle b \rangle)^2 \, p(a, b, \beta) \,, \tag{11}$$

$$cov(a,b) = \int d\beta \int da \int db \, (a - \langle a \rangle)(b - \langle b \rangle) \, p(a,b,\beta) \,, \tag{12}$$

where $\langle a \rangle = \int d\beta \int da \int db \ a \ p(a,b,\beta)$ and $\langle b \rangle = \int d\beta \int da \int db \ b \ p(a,b,\beta)$. The best-fit values of a and b determined by the maximum likelihood method along with Equations (5)-(7) as well as the associated errors and covariances estimated by Equations (10)-(12) for the six target groups are presented in Table 2.

We calculate the partial derivatives, $\partial r_t/\partial a$ and $\partial r_t/\partial b$ at $a=\hat{a}$ and $b=\hat{b}$, in Equation (9) and derive the following expressions.

$$\left(\frac{\partial r_t}{\partial a}\right)\Big|_{\hat{a},\hat{b}} = \frac{\hat{r}_t}{\hat{a}(1+\hat{b})}, \qquad \left(\frac{\partial r_t}{\partial b}\right)\Big|_{\hat{a},\hat{b}} = \frac{\hat{r}_t}{\hat{a}(1+\hat{b})}\ln\left(\frac{r_v}{\hat{r}_t}\right). \tag{13}$$

Through Equations (9)-(13), we finally estimate σ_{r_t} for each target group. It is worth emphasizing here that although the error on the nuisance parameter β , σ_{β} , does not explicitly appear in Equation (9), the variation of β is taken into full account for the determination

of the marginalized error, σ_{r_t} , since both of σ_a and σ_b are determined by the simultaneous marginalization of the posterior distribution, $p(a, b, \beta)$, over a, b and β .

Table 3 lists the estimated turn-around radii and the associated errors for the six targets, and compare the values with the spherical and non-spherical bound limits set by the Planck cosmology. As can be seen, for the cases of GG1, GG2, and GG3, the differences between \hat{r} and $r_{t,u}^{(s)}$ are larger than σ_{r_t} , while for the cases of GG4, GG5, and GG6, the differences fall within σ_{r_t} . Given this result, the former three groups could be regarded as candidates for the spherical bound limit violation. Yet, the comparison of $\hat{r}_t - r_{t,u}^{(ns)}$ with σ_{r_t} reveals that none of the six targets violate the non-spherical bound-limit.

4. Summary and Discussion

Employing the TRE algorithm developed by Lee et al. (2015b), we have estimated the turn-around radii of six isolated galaxy groups with masses in the range of $0.3 \le M_v/[10^{14}h^{-1}M_\odot] \le 1$ at redshifts of $z \le 0.05$ from the SDSS DR10. To ensure the validity and efficacy of the TRE algorithm, our analysis has been restricted to the local isolated galaxy groups around which the neighbor field galaxies exhibit anisotropic spatial distributions. For each of the six targets, we have constructed a radial velocity profile along the anisotropic distribution of the neighbor field galaxies (Figures 3-8) and fitted it to the analytic formula derived by Falco et al. (2014). Finally, the turn-around radius of each target has been determined as the radial distance at which the best-fit formula hits zero, and the marginalized errors propagated through the fitting procedure has been also evaluated (Table 3).

The measured turn-around radii of the six targets have been compared with the spherical and non-spherical upper bound limits predicted by the Λ CDM cosmology. Among the six targets, three have been shown to violate the spherical bound-limit, while the other three abide by it. Although no violation of the non-spherical bound limit is found, we have noted that the observed frequency at which the spherical bound violation occurs on the galaxy group scale is rather high compared with the numerical result of Lee & Li (2017) who found the frequency as low as 14% in a Λ CDM universe. Yet, before rushing to a conclusion that our observational result challenges the Λ CDM cosmology, it should be worth inspecting a more mundane source of this rather high frequency of the occurrence of the spherical bound-limit violation.

The first suspicion falls on the underestimate of the spherical bound limit caused by substituting the virial mass for the turn-around mass in Equation (1). Although it has been

presumed throughout our current analysis that for the case of the isolated galaxy group the virial mass would approximate well the turn-around mass, it has yet to be quantitatively addressed how close the virial mass of each target is to its turn- around mass, how the difference between the two masses would depend on the mass scale, and how significantly the difference would change the value of the spherical bound limit.

Another factor that has not been taken into account but may have contaminated the final result is the uncertainties associated with the measurements of the virial masses of the galaxy groups. Tempel et al. (2014) measured the virial masses of the SDSS groups under the assumption that the DM density profiles are well described by the universal NFW formula (Navarro et al. 1997). However, several numerical experiments already invalidated the concept of the universality of the NFW density profile (e.g., Navarro et al. 2004). The deviation of the true density profiles from the NFW formula may have caused systematic errors in the measurements of the virial masses of the target groups, which may have in turn contaminated our estimates of their turn-around radii.

The other downside is the small size of our sample consisting only of six target groups, which obstructs a statistically conclusive interpretation of the final result. This small sample size is an inevitable outcome of the generic limitation of the TRE algorithm which is applicable only to those isolated groups having web-like structures in their neighbor zones. Furthermore, since a web-like structure had to be identified from the anisotropic spatial distribution of the *field* galaxies to guarantee its gravitational link with the target, each identified web-like structure has turned out have a very low richness, which incurred inaccuracy in the construction of the radial velocity profiles. Our future work will be in the direction of addressing these remaining issues and improving further the statistical analysis as well as the TRE algorithm.

The manuscript has been significantly improved from the original version through revision thanks to many valuable suggestions from an anonymous referee. I acknowledge the support of the Basic Science Research Program through the National Research Foundation (NRF) of Korea funded by the Ministry of Education (NO. 2016R1D1A1A09918491). I was also partially supported by a research grant from the NRF of Korea to the Center for Galaxy Evolution Research (No.2017R1A5A1070354).

REFERENCES

Ahn, C. P., Alexandroff, R., Allende Prieto, C., et al. 2014, ApJS, 211, 17

Albaek, L., Hansen, S. H., Martizzi, D., Moore, B., & Teyssier, R. 2017, arXiv:1708.04822

Bernardeau, F. 1994, ApJ, 427, 51

Boylan-Kolchin, M., Springel, V., White, S. D. M., Jenkins, A., & Lemson, G. 2009, MNRAS, 398, 1150

Brinckmann, T., Lindholmer, M., Hansen, S., & Falco, M. 2016, JCAP, 4, 007

Falco, M., Hansen, S. H., Wojtak, R., et al. 2014, MNRAS, 442, 1887

Joyce, A., Jain, B., Khoury, J., & Trodden, M. 2015, Phys. Rep., 568, 1

Karachentsev, I. D., Tully, R. B., Wu, P.-F., Shaya, E. J., & Dolphin, A. E. 2014, ApJ, 782,

Kim, S., Rey, S.-C., Bureau, M., et al. 2016, ApJ, 833, 207

Klypin, A., Yepes, G., Gottlöber, S., Prada, F., & Heß, S. 2016, MNRAS, 457, 4340

Lee, J., Kim, S., & Rey, S.-C. 2015a, ApJ, 807, 122

Lee, J., Kim, S., & Rey, S.-C. 2015b, ApJ, 815, 43

Lee, J. 2016, ApJ, 832, 123

Lee, J., & Yepes, G. 2016, ApJ, 832, 185

Lee, J. 2017, ApJ, 839, 29

Lee, J., & Li, B. 2017, ApJ, 842, 2

Navarro, J. F., Frenk, C. S., & White, S. D. M. 1997, ApJ, 490, 493

Navarro, J. F., Hayashi, E., Power, C., et al. 2004, MNRAS, 349, 1039

Pavlidou, V., Tetradis, N., & Tomaras, T. N. 2014, JCAP, 5, 017

Pavlidou, V., & Tomaras, T. N. 2014, JCAP, 9, 020

Pearson, D. W., Batiste, M., & Batuski, D. J. 2014, MNRAS, 441, 1601

Planck Collaboration, Ade, P. A. R., Aghanim, N., et al. 2014, A&A, 571, A16

Tempel, E., Tamm, A., Gramann, M., et al. 2014, A&A, 566, A1

Tully, R. B., & Trentham, N. 2008, AJ, 135, 1488

Tully, R. B. 2015, AJ, 149, 54

Wall, J. V., & Jenkins, C. R. 2012, Practical Statistics for Astronomers, (Cambridge, UK: Cambridge University Press)

This preprint was prepared with the AAS LATEX macros v5.2.

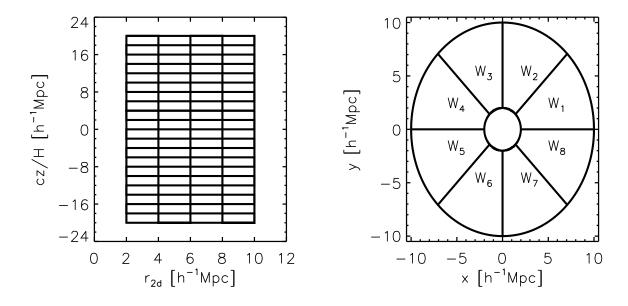


Fig. 1.— (Left panel:) Illustration of the pixelation of the bound zone around an isolated group in two dimensional space spanned by r_{2d} and cz/H, where r_{2d} is the separation distance from the group center in the plane of sky perpendicular to the line of sight toward the group. (Right Panel:) Illustration of the division of the plane of the sky around each isolated group into eight wedges of equal area.

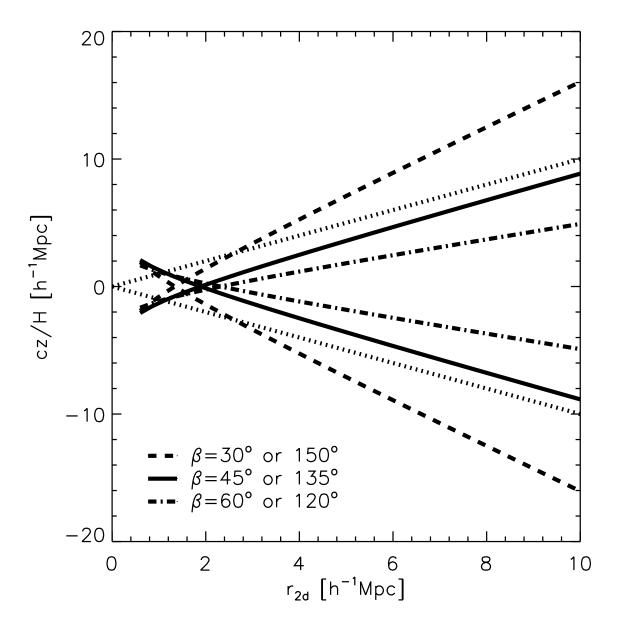


Fig. 2.— Projected radial velocity profiles of the bound-zone galaxies around a galaxy group with viral mass of $5 \times 10^{13} \, h^{-1} M_{\odot}$ for six different cases of the inclination angle, β .

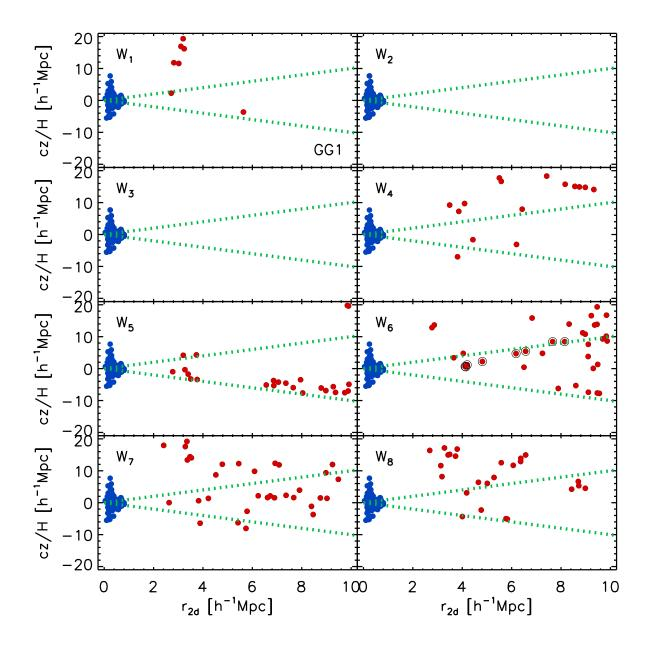


Fig. 3.— Configurations of the field galaxies (filled red dots) located in the overdense sites around an isolated galaxy group, GG1 (blue dots) from the catalog of Tempel et al. (2014). The open black dots indicate those field galaxies belonging to a web-like structure identified around GG1.

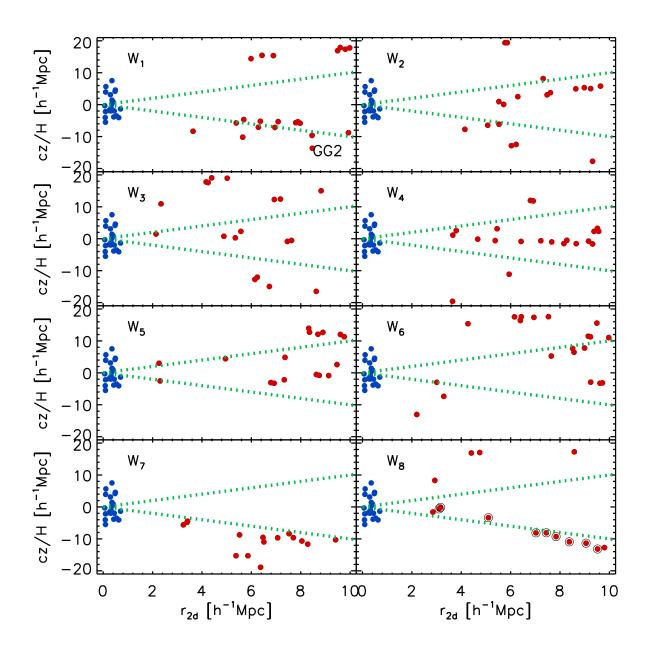


Fig. 4.— Same as Figure 3 but for a different galaxy group, GG2.

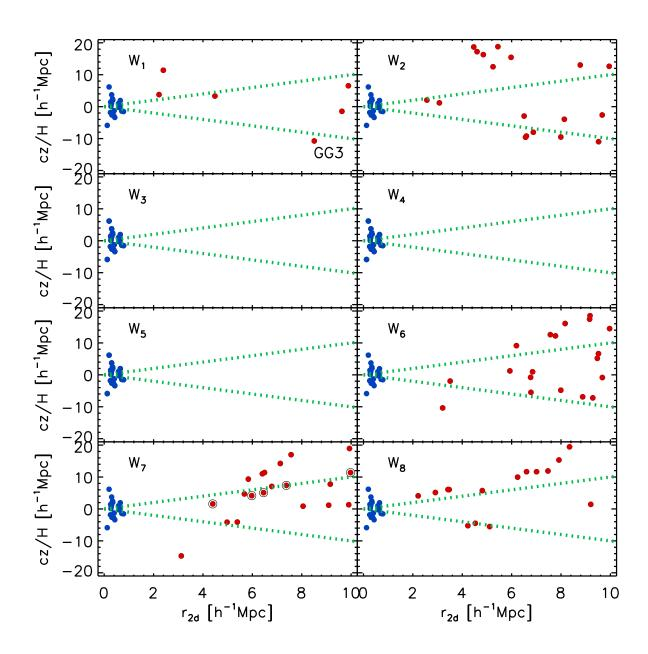


Fig. 5.— Same as Figure 3 but for a different galaxy group, GG3.

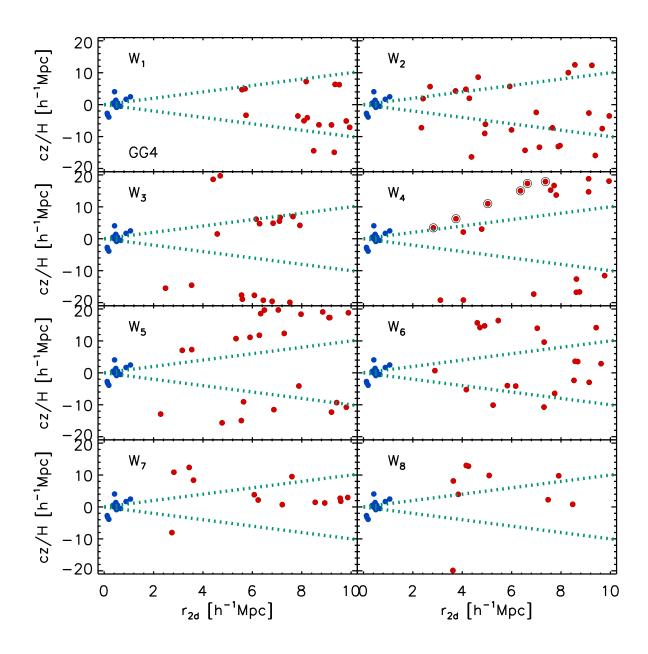


Fig. 6.— Same as Figure 3 but for a different galaxy group, GG4.

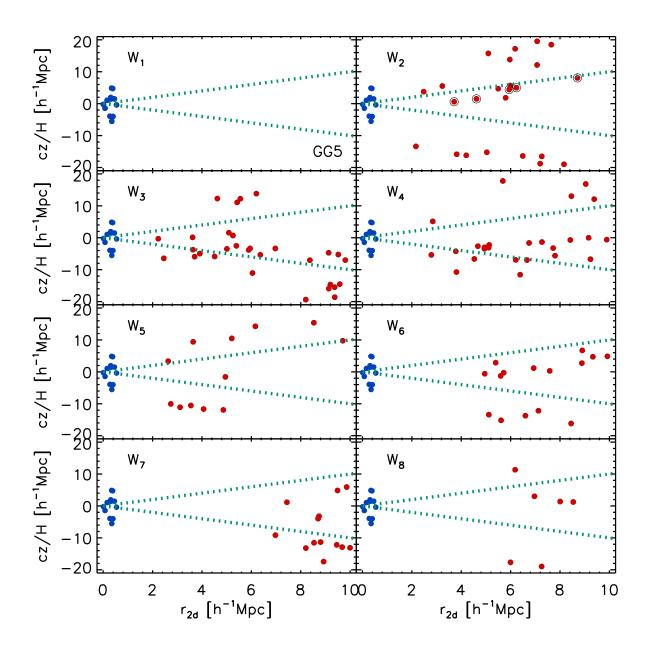


Fig. 7.— Same as Figure 3 but for a different galaxy group, GG5.

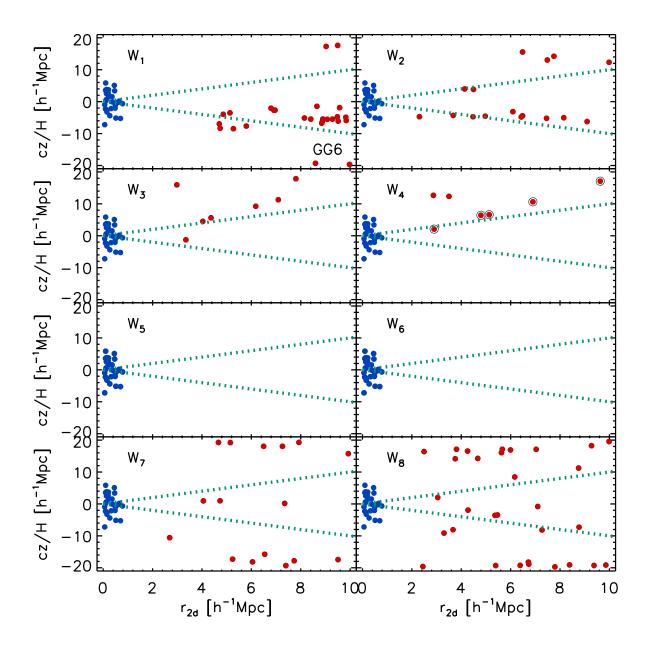


Fig. 8.— Same as Figure 3 but for a different galaxy group, GG6.

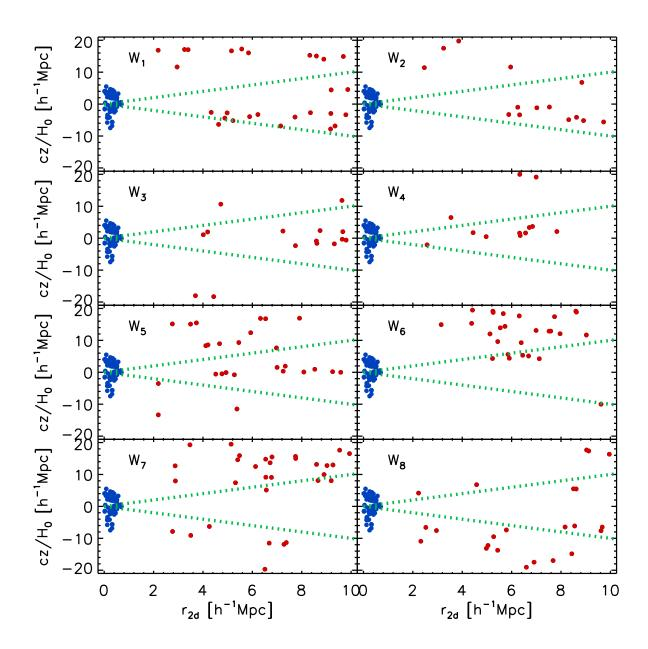


Fig. 9.— Same as Figure 3 but for a target group in the neighbor zone of which no web-like structure of the field galaxies is identified.

Table 1. Equatorial coordinates, redshifts, virial masses of the target groups

Group	<i>RA</i> (°)	DEC (°)	z	$M_v \\ (10^{12} h^{-1} M_{\odot})$
GG1	226.08	1.64	0.007	40.85
GG2	144.43	17.06	0.029	60.69
GG3	157.20	8.59	0.049	37.00
GG4	226.81	9.59	0.045	30.13
GG5	254.37	27.35	0.037	48.72
GG6	123.70	55.16	0.033	48.85

Table 2. Best-fit parameters and their covarances for the target groups

Group	\hat{a}	σ_a	\hat{b}	σ_b	cov(a,b)
GG1	1.13	0.32	-0.13	0.25	0.06
GG2	3.67	1.49	0.44	0.16	0.03
GG3	2.37	0.58	0.23	0.29	0.16
GG4	3.77	1.11	0.43	0.37	0.37
GG5	6.20	1.61	0.82	0.43	0.64
GG6	0.37	0.07	-0.39	0.16	0.01

Table 3. Turn-around radii of the target groups and the spherical and non-spherical bound limits

Group	$ \hat{r}_t \\ (h^{-1}\mathrm{Mpc}) $	$\frac{\sigma_{r_t}}{(h^{-1}\mathrm{Mpc})}$	$r_{t,u}^{(s)} \\ (h^{-1}\mathrm{Mpc})$	$r_{t,u}^{(ns)} \\ (h^{-1}\mathrm{Mpc})$
GG1	9.01	4.47	3.86	5.01
GG2	7.72	2.85	4.40	5.72
GG3	6.94	2.96	3.73	4.85
GG4	6.34	3.03	3.49	4.53
GG5	5.42	2.23	3.95	5.92
GG6	4.89	1.26	4.09	5.32